Impact of bias correction to reanalysis products on simulations of North American soil moisture and hydrological fluxes

Aaron A. Berg and James S. Famiglietti
Department of Earth System Science, University of California, Irvine, California, USA

Jeffrey P. Walker
Department of Civil and Environmental Engineering, University of Melbourne, Parkville, Victoria, Australia

Paul R. Houser
Hydrological Sciences Branch, NASA Goddard Space Flight Center, Greenbelt, Maryland, USA

Received 19 December 2002; revised 18 March 2003; accepted 13 April 2003; published 19 August 2003.

[1] Simulating land surface hydrological states and fluxes requires a comprehensive set of atmospheric forcing data at consistent temporal and spatial scales. At the continental-to-global scale, such data are not available except in weather reanalysis products. Unfortunately, reanalysis products are often biased due to errors in the host weather forecast model. This paper explores whether the error in model predictions of the initial soil moisture status and hydrological fluxes can be minimized through a bias reduction scheme to the European Centre for Medium Range Weather Forecast and National Center for Environmental Prediction/National Center for Atmospheric Research reanalysis products. The bias reduction scheme uses both difference and ratio corrections based upon global observational data sets. Both the corrected and original forcing data were used to simulate land surface states and fluxes with a land surface model (LSM) over North America. Soil moisture, snow depth, and runoff output from the LSM are compared to observations to assess the impact of the bias correction on simulation accuracy. Results of this study demonstrate the sensitivity of LSMs to bias in the forcing data, and that implementation of a bias reduction scheme reduces errors to the simulation of soil moisture, runoff, and snow water equivalence. Accordingly, the initial soil moisture fields produced should be more representative of actual conditions, and therefore more useful to the climate modeling community. Results suggest that modelers using reanalysis products for forcing LSMs, in particular for the establishment of initial conditions, should consider a bias reduction strategy when preparing their input forcing fields. *INDEX TERMS:* 1833 Hydrology: Hydroclimatology; 1836 Hydrology: Hydrologic budget (1655); 1866 Hydrology: Soil moisture; *KEYWORDS:* land surface modeling, hydroclimatology, soil moisture, reanalysis, hydrometeorological forcing

Citation: Berg, A. A., J. S. Famiglietti, J. P. Walker, and P. R. Houser, Impact of bias correction to reanalysis products on simulations of North American soil moisture and hydrological fluxes, *J. Geophys. Res.*, *108*(D16), 4490, doi:10.1029/2002JD003334, 2003.

1. Introduction

[2] After sea surface temperature, land surface soil moisture is the most important atmospheric boundary condition impacting climate [*Dirmeyer et al.*, 1999], and numerous studies [e.g., *Oglesby*, 1991; *Atlas et al.*, 1993; *Bounouna and Krishnamurti*, 1993a, 1993b; *Delworth and Manabe*, 1993; *Xue and Shukla*, 1993; *Milly and Dunne*, 1994; *Koster and Suarez*, 1996a; *Fennessy and Shukla*, 1999; *Douvill and Chavin*, 2000; *Ducharne and Laval*, 2000; *Koster et al.*, 2000a] have demonstrated the sensitivity of climate model simulations to soil moisture initialization. Given the importance of the soil moisture state for weather and climate prediction, numerous studies have identified techniques to observe soil moisture from remote sensing platforms [*Owe and Van de Griend*, 1998; *Jackson et al.*, 1999; *Rodell and Famiglietti*, 1999; *Owe et al.*, 2001], or produce data sets of initial land surface soil moisture for use in General Circulation Model (GCM) simulations of weather or climate [*Dirmeyer et al.*, 1999].

[3] Unfortunately, microwave remote sensing of soil moisture will provide information for only the top few centimeters and will be limited to areas of low to moderate vegetation foliage [*Njoku and Entekhabi*, 1996]. Therefore any attempt to produce a large-scale soil moisture data set must be realized through modeling only (over regions where data are not available) and where data are available through modeling with data assimilation strategies [e.g., *Houser et al.*, 1998; *Reichle et al.*, 2001; *Walker and Houser*, 2001; *Walker et al.*, 2001]. Hence a prerequisite for accurate

0148-0227/03/2002JD003334$09.00

simulations of the energy and mass fluxes between the atmosphere and land surface is comprehensive data sets of land surface and atmospheric properties. Despite great improvements to weather forecast models and to observation systems, the necessary atmospheric information over large areas of the globe is not available at the temporal and spatial scales required by the majority of land surface parameterization schemes. Thus over these regions, reanalysis products may offer the only source of the necessary climate information.

[4] Global weather forecast models, observational data streams, observation retrieval algorithms, and data assimilation techniques change with time, therefore, weather forecasting centers periodically rerun their forecast system with consistent models, observational data, and data assimilation strategies producing a "reanalysis." Although observations are assimilated into the reanalyses, model output should be treated with skepticism because many of the meteorological fields forecasted are only weakly constrained to model input [*Kalnay et al.*, 1996]. Bias in reanalysis products has been the subject of much research [*Betts et al.*, 1996, 1998a, 1998b, 1998c; *Maurer et al.*, 2001a, 2001b; *Roads and Betts*, 2000], and hence using reanalysis forcing to drive offline land surface models (LSMs) can result in unrealistic estimates of energy, mass, and momentum exchanges between the land and atmosphere [*Lenters et al.*, 2000; *Maurer et al.*, 2001a].

[5] Recognizing the existence of errors in the reanalysis products and their potential to impact offline LSM simulations, this paper presents a simple methodology for bias correction of reanalysis products. The bias correction methodology is applied to the European Centre for Medium Range Weather Forecasts (ECMWF) 15-year reanalysis (ERA) [*Gibson et al.*, 1997] and to the National Center for Environmental Prediction/National Center for Atmospheric Research (NCEP/NCAR) reanalysis (NRA) [*Kalnay et al.*, 1996]. The sensitivity of the bias correction scheme is assessed for large-scale soil moisture prediction over the North American continent. Further, the necessity of the bias correction is examined through comparisons with simulation results and observations from the Mississippi River basin. Simulations completed with each of the reanalysis products and the corrected reanalysis products are compared to runoff, soil moisture, and snow water equivalence (SWE) observations to highlight potential improvements to land surface simulation accuracy due to the bias correction. The Mississippi River basin is selected as the comparison region in this study due to the availability of observational data sets and abundance of previous studies [e.g., *Maurer et al.*, 2001a, 2001b; *Roads and Betts*, 2000]. Results of this study have implications for the sensitivity of land surface parameterization schemes to differences and errors in input forcing, and hence for the use of reanalysis products as forcing in uncoupled simulations of land surface energy and mass exchange.

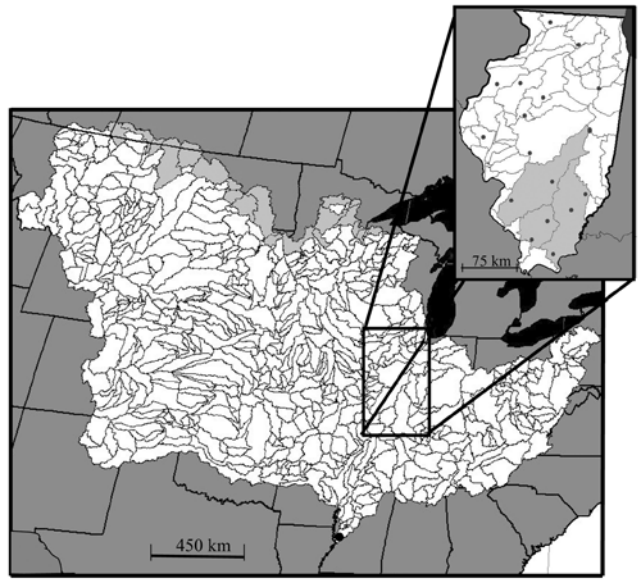

Figure 1. Catchment representation is shown over the Mississippi River above Vicksburg, Mississippi. Catchments used for the comparisons of snow depths over the northern portion of the basin are lightly shaded. The inset illustrates the soil moisture sampling stations within Illinois and the catchments (also lightly shaded) used for comparisons with the Illinois station data.

2. Models and Data Sets

2.1. Catchment-Based Land Surface Model

[6] This study makes use of the catchment-based LSM (CLSM) developed by *Koster et al.* [2000b]. The CLSM requires atmospheric forcing (short and longwave downwelling radiations, convective and total precipitation, 2-m air and dew point temperatures, 10-m wind speed, and surface pressure) together with surface parameter descriptions (vegetation type, height, greenness, leaf area index, roughness length at the surface, albedo, and the soil hydrologic properties) to perform calculations of soil water content, SWE, runoff, evapotranspiration, surface temperature, and the sensible and latent heat fluxes. A detailed model description is provided by *Koster et al.* [2000b] and *Ducharne et al.* [2000].

[7] Based in part on earlier work by *Famiglietti and Wood* [1991, 1994] and *Stieglitz et al.* [1997], an important feature of this LSM is the representation of spatially varying topography to allow for the parameterization of downslope flow and spatial variability in soil moisture, runoff, and surface fluxes. An important and unique feature of this model is the discretization of the land surface into watersheds (examples of the catchments over the Mississippi River basin are shown in Figure 1). Thus catchments form the fundamental computational element rather than the standard atmospheric grid.

[8] The energy balance equations of the CLSM closely follow those of *Koster and Suarez* [1992, 1996b], which are based on the Simple Biosphere (SiB) model of *Sellers et al.* [1986]. Vegetation types are specified to one of the eight types defined in the Mosaic LSM [*Koster and Suarez*, 1996b]. The snow model coupled to the CLSM parallels that of *Lynch-Stieglitz* [1994] and its interaction with the simulated water and energy balance is described by *Stieglitz et al.* [2001].

2.2. European Centre for Medium-Range Weather Forecasts and National Centers for Environmental Prediction/National Center for Atmospheric Research Reanalyses

[9] The ECMWF produced a 15-year reanalysis for the period 1979–1993 archived every 6 hours [*Gibson et al.*,

Table 1. Observational Data Sets Used to Perform Bias Correction to the Reanalysis and to Compare Simulation Results With Observations[a]

Reanalysis Field	Observed Data Set Used	Resolution	
		Temporal	Spatial
	Data Sets Used for Bias Correction of the Reanalysis		
2-m Air temperature	Climate Research Unit [*New et al.*, 2000]	monthly 1979–1993	0.5° × 0.5°
	Center for Climatic Research [*Legates and Willmott*, 1990]	monthly 1979–1993	0.5° × 0.5°
2-m Dew point temperatures	Climate Research Unit [*New et al.*, 2000]	monthly 1979–1993	0.5° × 0.5°
Precipitation	Global Precipitation Climatology Project Version 2 [*Huffman et al.*, 1997]	monthly 1979–1993	2.5° × 2.5°
Long and shortwave radiation	Langley Eight Year Shortwave and Longwave Surface Radiation Budget [*Gupta et al.*, 1999]	monthly 1983–1991	1.0° × 1.0°
		Resolution	
Hydrological Variable	Observed Data Set Used	Temporal	Spatial
	Data Sets Used for Comparisons With the Simulated Hydrologic Cycle		
Soil moisture	Illinois soil moisture [*Hollinger and Isard*, 1994]	biweekly 1980–1996	19 locations in Illinois
Runoff	U.S. Geological Survey Gauge 0728900 at Vicksburg, Mississippi	daily 1979–1993	
Snow depth	SMMR derived snow depth [*Chang*, 1995]	1978–1987	0.5° × 0.5°

[a]Note that the time frames given here reflect those used in the bias correction and are not necessarily those of the actual data set.

1997]. The forecast model includes 31 vertical levels and has a horizontal resolution of N80 (which corresponds to an approximate resolution of 1.125°). Differences between the ERA and observations are discussed by *Betts et al.* [1998a, 1998b, 1998c], *Roads and Betts* [2000], and summarized in section 4.1.

[10] The NRA is a long-term reanalysis (1948 to present) archived every 6 hours with a resolution of T62 (which corresponds to an approximate resolution of 1.875°) [*Kalnay et al.*, 1996]. There are several well-known deficiencies within the NRA model output including: a large overestimation of precipitation over the Mississippi basin, a consistent overestimation of evapotranspiration, and an underprediction of snow [*Maurer et al.*, 2001a]. Further comparisons between the NRA and observations are discussed by *Betts et al.* [1996], *Maurer et al.* [2001a, 2001b], *Roads and Betts* [2000], and summarized in section 4.1.

2.3. Observation-Based Data Sets

[11] We compiled two categories of data sets for use in this study. These include the global climate observations (temperature, precipitation, and radiation) used for the correction of the reanalysis products and surface hydrologic data used for comparison with CLSM simulations. Initial discussion is focused on the data sets assembled for bias correction of the reanalysis fields. Table 1 is a summary of the data sets used in this study.

[12] Bias correction of reanalysis 2-m air temperatures was made with an average of two data sets: the extended version (1.01) of *Legates and Willmott* [1990] and the Climate Research Unit half-degree (CRU-05) temperature grid [*New et al.*, 2000]. The resolution for both data sets is global at 0.5°. Key distinctions between the two data sets include data sources and interpolation methodologies.

[13] Bias correction of reanalysis short and longwave radiations was performed to the Langley 8-Year Surface Radiation Budget (SRB) developed by the Radiation Sciences Branch of the Atmospheric Sciences Division at NASA's Langley Research Center [*Gupta et al.*, 1999].

[14] Monthly mean downward and net radiation at the surface is divided into two spectral regions, shortwave (0.2–5.0 μm) and thermal longwave (5–50 μm). The SRB data set, which spans the period July 1983–June 1991, is model derived, based on observations from the International Satellite Cloud Climatology Project (ISCPP) [*Gupta et al.*, 1999].

[15] Reanalysis precipitation was corrected to the Global Precipitation Climatology Project (GPCP) Version 2 Combined Precipitation Data set developed by the NASA Goddard Space Flight Center's Laboratory for Atmospheres [*Huffman et al.*, 1997]. The GPCP spans the period January 1979-present on a 2.5° × 2.5° grid. Precipitation estimates derived from low-orbit-satellite microwave sensors, geosynchronous-orbit-satellite infrared sensors, and rain gauges were used to create the data set [*Huffman et al.*, 1997].

[16] For the comparison of CLSM simulations with observations, data sets were obtained for soil moisture, runoff, and SWE for regions within the Mississippi River basin. A data set of soil moisture observations taken over the state of Illinois [*Hollinger and Isard*, 1994] was obtained through the Global Soil Moisture Databank [*Robock et al.*, 2000]. The Illinois soil moisture data set includes observations obtained from 19 sites. The observations are either biweekly (March–September) or monthly (October–February) for 11 depths (0–10, 10–30, 30–50, 50–70, 70–90, 90–110, 110–130, 130–150, 150–170, 170–190, and 190–200 cm). To compare the soil moisture observations with the CLSM generated root zone soil moisture (top 1 m), the average moisture content in the top 100 cm of soil was determined for a group of measurement stations in southern Illinois (see inset of Illinois in Figure 1). These stations were selected as they are spread among three contiguous catchments with at least two stations for each catchment represented. Unfortunately, the station records do not always follow a regular collection interval, and periods of missing data are common. Therefore a monthly average for the three-catchment region was determined using all the available data.

[17] Further comparisons of CLSM water balance simulations were examined for runoff and SWE. We compare river runoff simulations to observations obtained from the United States Geological Survey (USGS) for gauge 07289000 at Vicksburg, Mississippi. The catchments upstream of the Vicksburg stream gauge are shown in Figure 1.

[18] Monthly CLSM simulations of SWE are compared with observations from the Nimbus-7 Scanning Multichannel Microwave Radiometer (SMMR) Derived Global Snow Cover and Snow Depth Data set available from the National Snow and Ice data center [*Chang*, 1995; *Chang et al.*, 1992]. For the SMMR period (November 1978 to August 1987), the data set is global in coverage on a 0.5° latitude by 0.5° longitude grid. The algorithm calculates snow depth by considering the difference in brightness temperatures between the 37 and 18 GHz channels and assuming constant snow density and grain size [*Chang et al.*, 1987]. The methodology works best over uniform regions such as the Canadian high plains, as the signal can be impacted by snow liquid water content, crystal size, snow depth, stratification, surface roughness, snow density, snow temperature, soil moisture, and vegetation cover [*Chang et al.*, 1987]. Hence for comparisons with simulated SWE, only catchments across the north of the Mississippi basin were used (see Figure 1). In these catchments, observational errors associated with high vegetation cover and complex topography are expected to be minimal. Before comparisons with simulated SWE the snow depth observations were converted to SWE based on the snow density reported by *Chang et al.* [1987]. It should also be noted that snow depths calculated from SMMR are typically 10% lower than estimates from earlier ground-based products, as microwave sensors cannot detect snow less than 5 cm deep [*Chang et al.*, 1987].

3. Methods

[19] The necessary climate inputs into the CLSM are short and longwave downwelling radiations, convective and total precipitation, 2-m air and dew point temperatures, 10-m wind speed, and surface pressure. The reanalysis products supply the necessary data at 0000, 0600, 1200, and 1800 UT, and the six hourly forcing data is interpolated by the CLSM into 20-min time steps. The methodology of the bias correction described in this section ensures that the necessary climate inputs are in agreement with the observational record at the monthly timescale. Problems with the diurnal cycles and intramonthly variability were not considered in this analysis, but should be addressed in future work.

[20] We describe two general types of bias correction: (1) a difference-based scheme, that adds or subtracts the estimated amount of bias from the affected forcing field and (2) a ratio-based scheme, which multiplies the affected forcing field by the ratio of monthly average reanalysis value to the observation value. The choice of the bias correction scheme was dependent on properties of the forcing field. For the correction of temperature, we used a difference-based approach to maintain the relative size of the diurnal cycle. Here a ratio-based approach may overly distort the size of the diurnal temperature range as recorded in the six hourly observations. Where zero values occurred in forcing fields (e.g., as in downwelling shortwave radiation and precipitation) a ratio-based approach was selected in order to obtain the monthly average without adding flux, obtaining negative values, or changing statistics such as the ratio of precipitation falling in one time period to the monthly total. Discussion of possible improvements to the approaches described below is included in section 5.

[21] Due to the limited availability of observational data sets, the bias reduction scheme was applied only for 2-m air and dew point temperatures, short and longwave downwelling radiations, and convective and total precipitation. Reanalysis-based surface pressure was adjusted to the catchment elevation, but not corrected to an observational product. We made no modifications to the wind speed. The total amount of convective rainfall was adjusted to match the ratio of convective to total precipitation predicted by reanalysis product (convective precipitation is treated differently in the CLSM than large-scale precipitation). Discussion below will focus on the interpolation procedures, forcing production, and the CLSM sensitivity experiments.

3.1. Interpolation Methodology

[22] A unique feature of the catchment-based LSM of *Koster et al.* [2000b] is the discretization of the land surface into catchments. This model formulation requires that the forcing data also be interpolated to the catchment space. Interpolating grids to catchments follows the methodology of *Koster et al.* [2000b] where the net flux (F) into catchment b is computed by:

$$F_n = \frac{\sum_g F_g A_{bg}}{\sum_g A_{bg}}, \tag{1}$$

where A_{bg} is fractional area of catchment b within grid cell g. For interpolation of the reanalysis data (which are considered as a sequence of nodes or grid points), we defined a quasi-rectangular grid surrounding each node (the quasi-rectangular grid corresponds to the reanalysis resolution of approximately 1.125° for the ECMWF and 1.875° for NCEP-NCAR). Next, we determined the area of each grid over the North American continent, and then interpolated the defined grids into catchment space using equation (1).

3.2. Temperature and Dew Point Temperature Corrections

[23] A single observational data set to bias correct the reanalysis 2-m air temperature was constructed by merging the 0.5° global mean monthly air temperature observations of the Climate Research Unit [*New et al.*, 2000] with the extended version of *Legates and Willmott* [1990], by simply averaging values from the two data sets. An elevation correction was then applied to the grid data by adjusting the observations, ERA and NRA 2-m air temperatures to sea level temperature, following the environmental lapse rate (6.5 K km^{-1}) and their respective reference elevations. This step is necessary to ensure that temperature differences due to changes in elevation across the various data sets were not included in the interpolation to catchment space. The elevations of the 0.5° observational grids were derived from TerrainBase 5′ Global Digital Terrain Model [*Row et al.*, 1995], a 5-min digital elevation model (DEM) of the Earth. The NRA and ERA grid points were reduced to sea level from their recorded geopotential heights. After the lapse rate correction, both observations and reanalysis data can be interpolated to catchment space following equation (1).

[24] Next, we applied a difference-based correction to the reanalysis fields as

$$\mathrm{Ta}_i = \mathrm{Ta}(R)_i + \left[\mathrm{Ta}(O) - \frac{\sum_{i=1}^{n} \mathrm{Ta}(R)_i}{n}\right]. \tag{2}$$

[25] Here Ta_i is the 2-m bias reduced air temperature (°K) at time step i, $Ta(R)_i$ is the 2-m reanalysis air temperature (°K), $Ta(O)$ is the average of the elevation reduced (shifted to sea level) CRU-05 and *Legates and Willmott*'s [1990] 2-m monthly average 0.5° air temperature observations (°K), and n is the number of time steps in a given month.

[26] The final step involved elevating the bias-corrected 2-m air temperatures to the catchment elevation following the environmental lapse rate where the catchment definitions and mean elevations were previously determined [*Verdin and Verdin*, 1999] from the 30-arc second digital elevation model GTOPO30 [*Gesch et al.*, 1999].

[27] To minimize bias in the reanalysis dew point temperatures, fields of average monthly relative humidity were constructed from vapor pressure and temperature estimates by *New et al.* [2000] and from the two reanalysis products. We did not use the vapor pressures of *New et al.* [2000] directly because in that study this field was classified as a secondary variable, signifying that it has been estimated using predictive relationships, and therefore we cannot place greater certainty on the estimates of New et al. than on the reanalysis products.

[28] Corrections to dew point temperatures were implemented in the following way. First, monthly average relative humidity was calculated for each of the reanalyses and the data set of *New et al.* [2000], before implementing the lapse rate elevation correction to monthly air temperature. From the three (monthly average) relative humidity fields we obtained an average, which was interpolated to catchment space. Next, the monthly average relative humidity field was used with air temperature observations (now corrected for bias and elevation) to evaluate a monthly average dew point temperature [following *Jensen et al.*, 1990]. We could then complete the bias correction to dew point temperature identically to equation (2), substituting dew point temperatures (Td) for Ta. For catchments where monthly observed dew points were higher than in the reanalysis, equation (2) was solved iteratively to reproduce the monthly average (Td(OBS)) while preventing Td_i from exceeding the corresponding Ta_i.

3.3. Corrections to Longwave and Shortwave Downwelling Radiations

[29] Bias correction to ERA and NRA short and longwave downward radiations was completed by a ratio-based correction to the Langley Shortwave and Longwave SRB data set [*Gupta et al.*, 1999], which was interpolated to a 1° × 1° grid and included as part of the Goddard Distribute Active Archive Center Climatology Interdisciplinary Data Collection. For the initial step in the bias correction, both of the reanalysis products and the SRB observations were interpolated to catchment space following equation (1).

[30] Next, a ratio-based bias correction to the reanalysis shortwave downward radiation ($S\downarrow$) was completed as:

$$S\downarrow_i = \frac{S\downarrow(O)}{\left(\frac{\sum_{i=1}^{n} S\downarrow(R)_i}{n}\right)} S\downarrow(R)_i, \tag{3}$$

where $S\downarrow(O)$ is observed monthly shortwave downward radiation from the Langley SRB data set (W m^{-2}), and $S\downarrow(R)_i$ is shortwave downward radiation at the surface from the reanalysis product (W m^{-2}) at time i.

[31] To maintain consistency with the shortwave correction, an equation identical to equation (3) was applied for the bias correction to the longwave downwelling radiation ($L\downarrow$)

$$L\downarrow_i = \frac{L\downarrow(O)}{\left(\frac{\sum_{i=1}^{n} L\downarrow(R)_i}{n}\right)} L\downarrow(R)_i. \tag{4}$$

[32] The methodology of the bias correction described in this study is different from that used by the International Satellite Land Surface Climatology Project (ISLSCP) Initiative 1 [*Sellers et al.*, 1996], where the downwelling shortwave radiation was calculated using the observed and reanalysis net shortwave radiation (S_{net}) and albedo (α) derived by the reanalysis as follows

$$S\downarrow_i = \frac{S_{net}(O)}{\left(\frac{\sum_{i=1}^{n} S_{net}(R)_i}{\frac{n}{(1-\alpha)}}\right)} \times \left(\frac{S_{net}(R)_i}{(1-\alpha)}\right). \tag{5}$$

[33] This approach is problematic, particularly for the bias correction of the ERA, since the winter albedo values over the boreal forest regions of Canada were found to be incorrect [*Betts et al.*, 1998b]. A similar problem was introduced into the bias correction to longwave surface radiation in the methodology used by ISLSCP Initiative 1, where a ratio-based bias correction was applied to the net longwave radiation (L_{net}), and the upward longwave component was calculated based on the ERA surface temperature (Ts(R)), the surface emissivity (0.996), and the Stefan-Boltzmann constant (b) [*Sellers et al.*, 1996]

$$L\downarrow_i = \frac{L_{net}(O)}{\frac{\sum_{i=1}^{n} L_{net}(R)_i}{n}} L_{net}(R)_i + 0.996(b)\left[\frac{\mathrm{Ts}(R)_i + \mathrm{Ts}(R)_{i-1}}{2}\right]^4. \tag{6}$$

[34] This approach introduces the possibility of bias to the downwelling radiation in regions where surface temperatures are incorrectly forecast by the reanalysis products.

3.4. Corrections to Precipitation

[35] Total precipitation from the ERA and NRA was corrected to the monthly observations from the GPCP Version 2 Combined Precipitation Data Set [*Huffman et al.*, 1997]. Each of the data sets (GPCP and the reanalyses) was interpolated to catchment space using equation (1) and a ratio-based correction procedure applied

$$P_i = \frac{P_{obs}}{\left(\frac{\sum_{i=1}^{n} P(R)_i}{n}\right)} P(R)_i, \tag{7}$$

where P_i is the bias-corrected catchment-based precipitation (mm) at time i, and P_{obs} is the average monthly precipitation observations from GPCP (mm).

[36] Over several catchments, precipitation was recorded in GPCP observations, but not in the reanalysis product over the same month, thus making a ratio-based correction impossible. To correct precipitation over these catchments, a multiple logistic regression was performed using the variables, relative humidity and cloud cover. The result of the regression model is a coefficient representing the probability of precipitation for the 6-hour reanalysis time step. We could then apply precipitation over the catchment for the time step with the highest probability at a rate equivalent to the monthly median amount of 6-hourly precipitation multiplied by the probability coefficient. This process was repeated for the time step with the next highest probability until the monthly shortfall of precipitation over the catchment in question was overcome. Over a typical year, the logistic equation was applied over less than 8% of the total number of catchments. The final step in the precipitation correction procedure was to adjust the amount of convective precipitation to match the ratio of convective to total precipitation originally forecast by the reanalysis product.

3.5. Experimental Framework

[37] To evaluate the impact of the atmospheric forcing bias correction on soil moisture prediction and hydrologic flux simulation, the CLSM was run for the period 1985–1991 using the corrected ERA (CERA), the corrected NRA (CNRA), and the uncorrected versions of the ERA and the NRA forcing (both of which were interpolated to catchment space but otherwise unmodified). This time period was selected to maximize the overlap of the available observational (the main constraint was the time period of the SRB observations July 1983–June 1991) and reanalysis data sets. It is important to distinguish between the CLSM simulations driven with each of these forcing products, hereafter called the ERA, CERA, NRA, and CNRA simulations, in contrast to the fully coupled ERA and NRA model results themselves.

[38] We completed all simulations using an identical version of the CLSM and employing the same scheme for initialization by model spin-up. During model spin-up, the initial model states were determined by driving the model to equilibrium for the beginning of 1985 through repeated simulation of 1985. Therefore each simulation has a starting position in climatological equilibrium with its own forcing data, rather than beginning each simulation from an identical initial state. This decision was made to simulate the initial state values modelers would obtain by considering each of the forcing data sets independently, rather than a composite of all the available information (this could also be considered a typical scenario because few modeling studies consider more than one forcing data set). Output from the CLSM simulations for each of the forcing products was then compared both to each other and to observations for the time period 1985–1991.

4. Results and Discussion

4.1. Forcing Intercomparison

[39] In this section, we document differences between the reanalysis products and the observational data sets incorporated into the bias correction. The purpose of this is not to examine regional bias in the reanalysis products, as similar analyses have already been carried out by a number of other researchers [*Betts et al.*, 1998a, 1998b, 1998c; *Maurer et al.*, 2001a, 2001b]. However, some discussion of the differences between the reanalysis products and observation–based data sets is necessary to understand the impact of the bias correction on modeling skill. Therefore Figures 2 and 3 present average seasonal DJF (December, January, February) and JJA (June, July, August) differences (1985–1991) between the reanalysis products and the observational data sets incorporated into the bias correction.

[40] Differences between reanalysis air temperatures and observations incorporated into the bias correction are illustrated in Figures 2, 3a, and 3b. For both reanalyses, differences are greatest during the winter period. For DJF the ERA exhibits a large cold bias (illustrated as the large blue region) that surrounds Hudson's Bay. This bias, due to an error with the modeled albedo [*Betts et al.*, 1998b], disappears after snowmelt in May. Further discussion of this problem is presented by *Betts et al.* [1998b] and will not be repeated here. In contrast, the NRA exhibits a slight warm bias over this region during the same season, with a considerable warm bias over the mountainous regions of Alaska and Yukon Territory, Canada. Over mountainous topography scale differences between ERA (approximately 1.125°), the NRA (1.875°), and the catchments (approximately 0.5°) are large; this results in considerable differences to temperature based on elevation differences (or approximately 1°K for every 150-m difference in elevation). Likely some of the bias in NRA observed over the Rocky Mountains is due to scale differences, however, the individual contribution from topography and bias effects was not resolved.

[41] During the summer period, both reanalyses are closer to observations, although ERA (NRA) temperatures are positively (negatively) biased along the western portion of the continent. In both reanalyses, the cause of some of these discrepancies over the Rocky Mountains is due to the lapse rate correction discussed above.

[42] In Figures 2c, 2d, 3c, and 3d, differences between the reanalysis vapor pressure and the vapor pressure composite are presented. For the reanalyses, differences are low in winter, and in the ERA, low for both seasons. Although in the ERA, the effects of the topographic lapse rate correction may be evident in JJA over the Rocky Mountains. In Figure 3d, JJA differences between the NRA and the vapor pressure composite show much higher vapor pressures over the Boreal forests of Canada, extending southward into the southeast of the United States. This issue was addressed by *Betts et al.* [1996], who compared First ISLSCP Field Experiment (FIFE) data with NRA output. In their study, mixing ratios in the NRA were found to be moister than observations, particularly during the summer period. Over the Southwest United States, vapor pressures in the NRA are much lower than in the composite. This issue has not been addressed in previous literature, but a full examination of the underlying causes for this bias is beyond the scope of this paper.

[43] In Figures 2e–2h and 3e–3h, we present differences between the SRB, and the ERA and NRA long and shortwave downwelling radiations. For both reanalyses, downwelling longwave (shortwave) radiation is underesti-

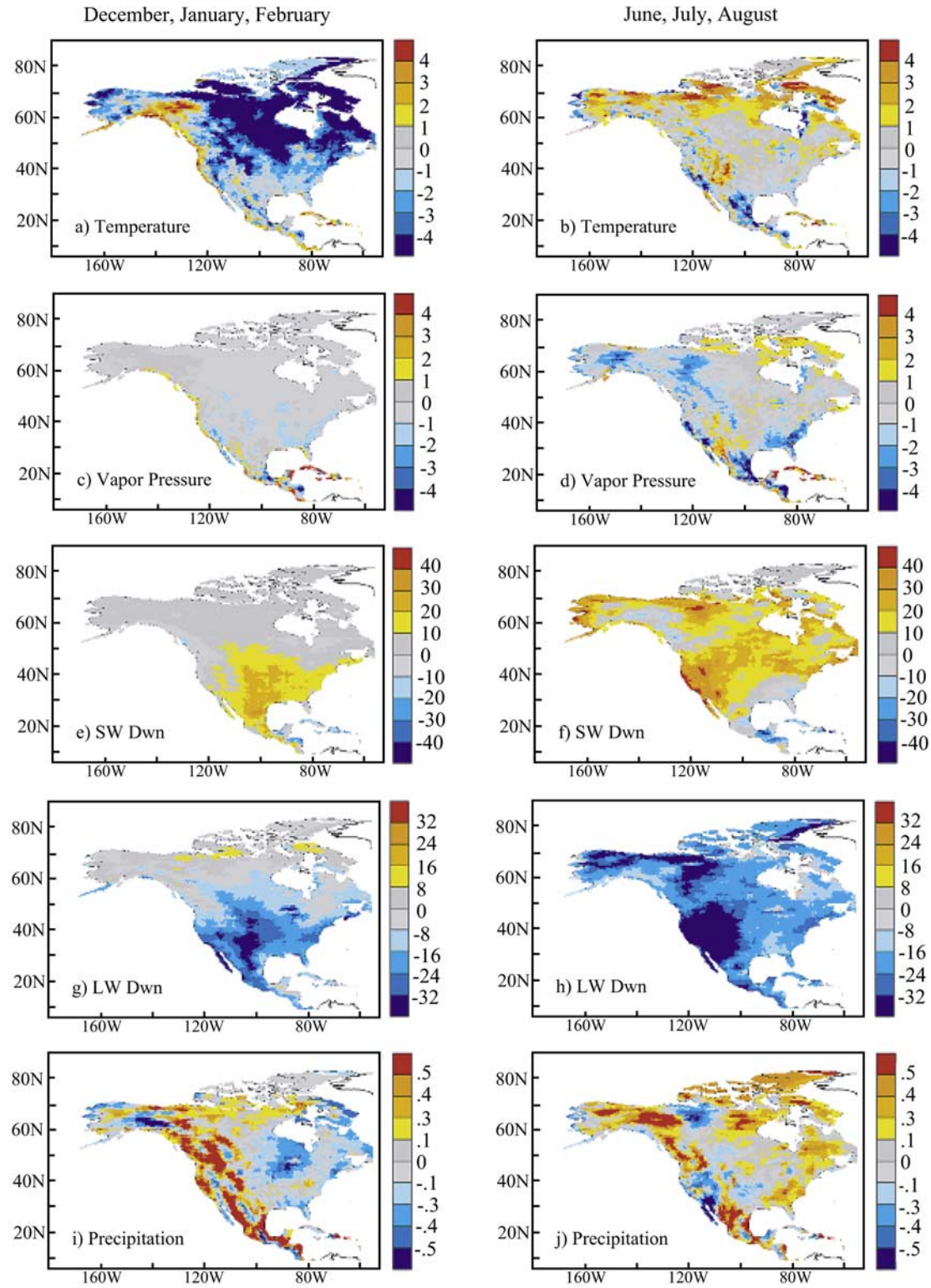

Figure 2. Seasonal (DJF and JJA) differences between the ERA and observations incorporated (ERA-observations) into the bias reduced forcing data set. Differences are for (a, b) air temperature (°C), (c, d) vapor pressure (hPa), (e, f) downwelling shortwave radiation (W m^{-2}), (g, h) downwelling longwave radiation (W m^{-2}), and (i, j) ratio of precipitation differences to total precipitation.

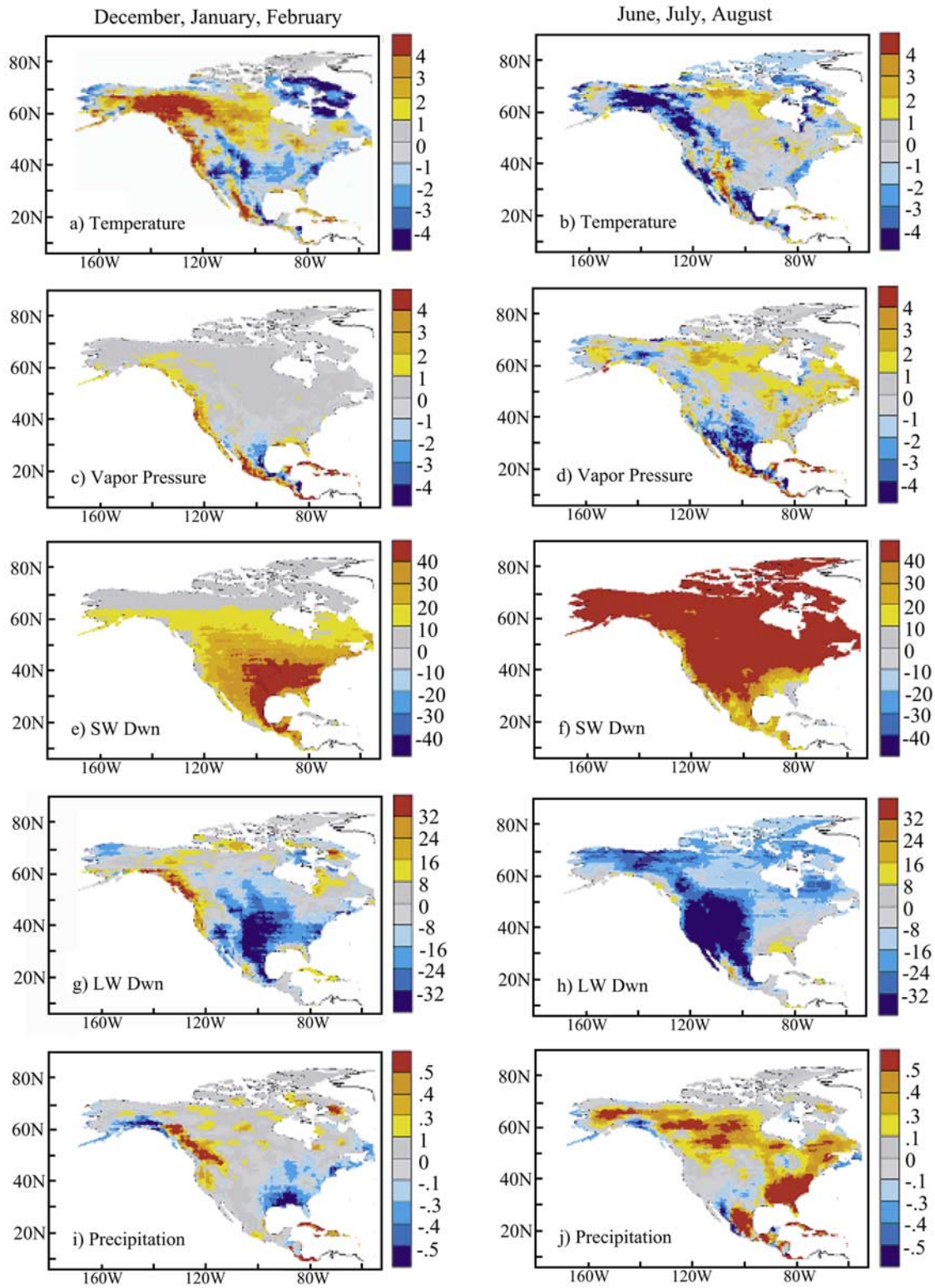

Figure 3. Seasonal (DJF and JJA) differences between the NRA and observations incorporated (NRA-observations) into the bias reduced forcing data set. Differences are for (a, b) air temperature (°C), (c, d) vapor pressure (hPa), (e, f) downwelling shortwave radiation (W m^{-2}), (g, h) downwelling longwave radiation (W m^{-2}), and (i, j) ratio of precipitation differences to total precipitation.

mated (overestimated). The differences between ERA and the SRB product, while high, are not out of the range, which is discussed in the work of *Wild et al.* [1998] and *Gupta et al.* [1999]. For the NRA, differences between the reanalysis downwelling shortwave and the SRB product are larger (approaching 40 W m^{-2} during the summer). Some discussion of this issue was presented by *Betts et al.* [1996], where the overestimation of shortwave radiation was found to be due to an overly transparent atmosphere and imperfect coupling scheme between cloud and radiation. Subsequently, on clear days downwelling shortwave radiation was up to 50 W m^{-2} higher than the FIFE station data [*Betts et al.*, 1998b].

[44] Figures 2i, 2j, 3i, and 3j display differences between the reanalysis and GPCP precipitation. Here we have plotted differences expressed as a ratio, where the difference between the monthly reanalyses and observations is divided by the observed total, thus normalizing the differences. This was done to illustrate the magnitude of bias with respect to the total amount of precipitation. For DJF, bias to ERA precipitation is positive (ERA greater than observations shown in red) over Rocky Mountains, and negative over the northern Mississippi basin extending northward to Hudson's Bay. In the summer period, regions of positive precipitation bias are observed over Alaska and in central Mexico. Over regions with high precipitation gradients, such as over the Rocky Mountains, bias in the reanalysis estimates are most likely exaggerated due to low resolution of the observational data set.

[45] In Figure 3i, positive bias in the NRA precipitation is observed over the Rocky Mountains north of the United States border, and a strong negative bias is observed in the southeast United States. In JJA, a belt of high precipitation bias is observed in the southeast United States extending north and westward across the Boreal forests of Canada. Bias in NRA precipitation is a well-known problem [e.g., *Roads and Betts*, 2000] and weaknesses to the precipitation parameterization scheme have been addressed [e.g., *Hong and Pan*, 1996] in subsequent reanalysis projects.

4.2. Simulations of Soil Moisture for the North American Continent

[46] Average simulated root zone volumetric soil moisture conditions for the JJA (1985–1991) period using the ERA, CERA, NRA, and CNRA forcing are presented in Figure 4. Overall, the patterns simulated by the ERA, CERA, and CNRA simulations are very similar, with only slight differences apparent over northwest Canada and Alaska, while the ERA simulation was typically wetter than both of the corrected simulations. As expected, regional differences between the ERA and the corrected data sets correspond to differences in the precipitation forcing. In contrast to the ERA, CERA, and CNRA simulations, mean summer soil moisture conditions predicted using the NRA forcing are much wetter (due to the precipitation and vapor pressure bias identified above). The regions of greatest difference occur over the southeast United States and extending northward and westward to the north of the Great Plains. It is interesting to note that although the CERA and CNRA simulations have identical monthly averages for air and dew point temperatures, downwelling radiation fields, and precipitation the CNRA simulation is slightly wetter than both CERA and ERA simulations east of the hundredth meridian and north over the Boreal forests of Canada (identical to the region of high precipitation bias in the NRA forcing). The reason for these differences is due to variability between the CERA and CNRA at submonthly and diurnal scales. The magnitude, seasonality, and impact of these differences on hydrological simulations are presently under investigation.

[47] Although the overall soil moisture pattern was similar for simulations completed with the ERA, CERA, and CNRA forcing, more pronounced regional differences occur over shorter periods and over different seasonal time frames (as opposed to the 7 year averages shown in Figures 4a–4d). To illustrate this point, in Figures 4e–4h we show average root zone differences between the ERA and the CERA (Figures 4e and 4f) and between NRA and CNRA (Figures 4g and 4h) for a single day (15 June 1987 and 15 June 1989). In all four plots, the regions over which a sizable precipitation bias was removed (areas greater than 0.5% or less than −0.5% in Figures 2i, 2j, 3i, and 3j) are observable over both dates. However, over regions of lower precipitation bias, the differences between simulations completed with the uncorrected reanalysis and their corrected counterparts are unique, suggesting different patterns of the initial soil moisture state. This is significant because differences in the spatial patterns of the initial soil moisture will affect climate prediction [*Dirmeyer*, 2000].

[48] The magnitude of differences between the simulated root zone soil moisture is also dependant upon the season of simulation. In Figure 5, we show continental average monthly (1985–1991) differences (for snow free catchments) between simulations of root zone soil moisture for the uncorrected (ERA and NRA) and corrected (CERA and CNRA) forcing data. Differences between the CERA and CNRA simulations are small (typically less than 1% cm^3 cm^{-3} for all seasons), with the CNRA simulation slightly wetter than the CERA simulation. In contrast, the differences between the ERA and CERA simulations, and the NRA and CNRA simulations, are much greater with the simulations from the noncorrected forcing data producing much wetter conditions than those from the corrected forcing data. Moreover, there are distinct seasonal cycles in the overall magnitude of difference that peaks over the winter period. In the discussion below, we will examine more closely the reasons for these differences and implications on hydrological flux simulations through comparisons with observations taken over the Mississippi River basin.

4.3. Comparison of Simulation Results With Observations From the Mississippi River Basin

4.3.1. Comparisons to Illinois Soil Moisture Observations

[49] To assess the improvement in simulated soil moisture due to the bias correction, Figure 6 presents simulated and observed root zone soil moisture for the catchments in southern Illinois (see Figure 1). The correlation and Mean Absolute Error (MAE) between observed and simulated soil moisture (January 1985–July 1991) are presented in Table 2. Overall, the ERA, CERA, and CNRA simulations accurately represent the observed seasonal cycle (wet in winter and early spring with a consistent dry down throughout the summer) with identical levels of correlation

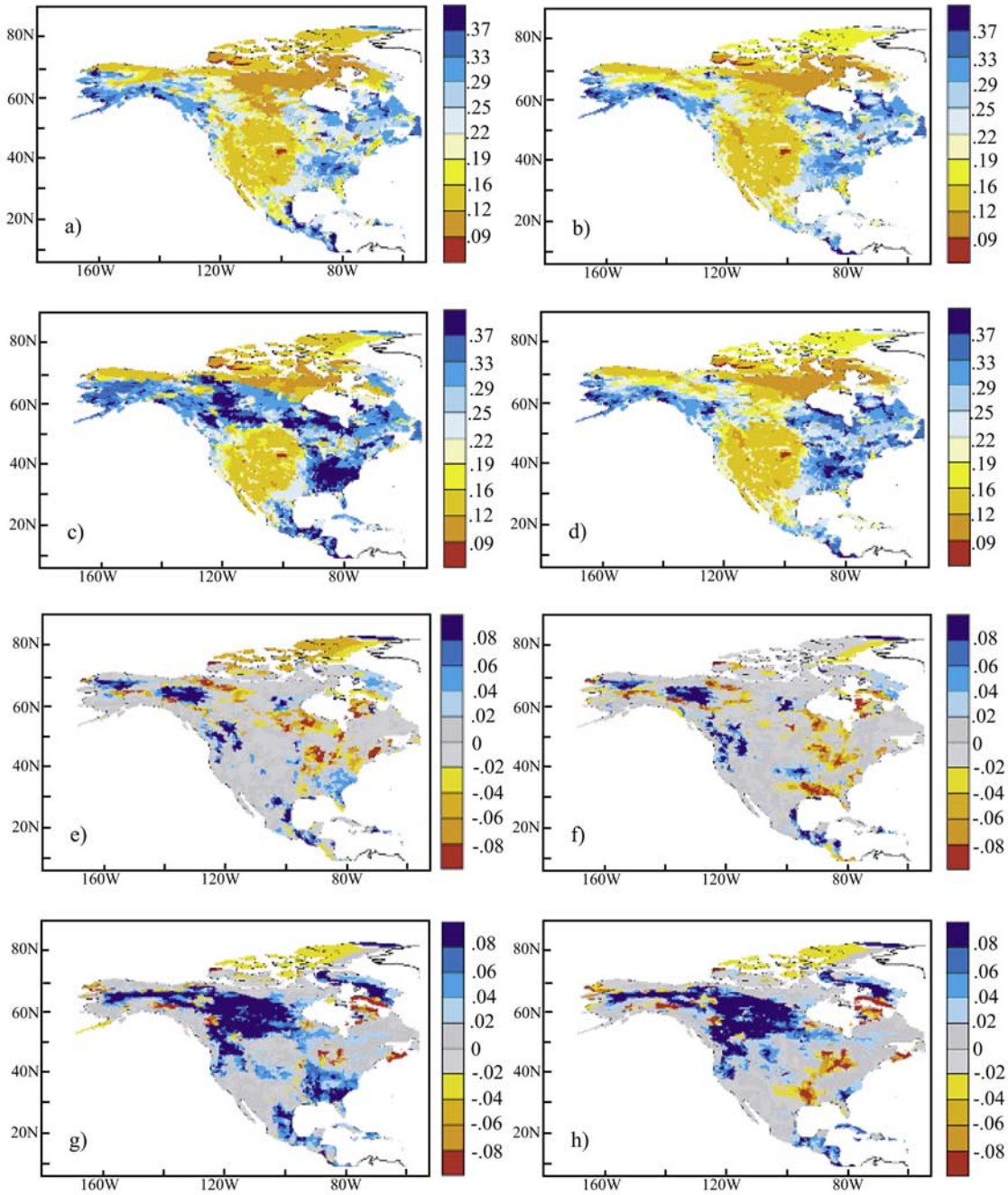

Figure 4. Average JJA (1985–1991) volumetric (cm^3 cm^{-3}) root zone soil moisture conditions for simulations completed with (a) ERA, (b) CERA, (c) NRA, and (d) CNRA forcing. (e, f) Differences between the ERA and CERA root zone soil moisture are shown for 15 June 1987 and 15 June 1989 and also (g, h) for the identical dates for differences between the NRA and CNRA.

and MAE calculated for the CERA and CNRA simulations. The dry down during the late spring through summer months is particularly well simulated. However, none of these simulations responds quickly enough to the observed increase in root zone soil moisture during the fall. Of the three simulations, the ERA responds the slowest (corresponding to the slightly lower levels of correlation and higher MAE). In contrast to the ERA, CERA, and CNRA simulations, correlations between the NRA simulation and observations are much weaker, and simulated root zone soil moisture is much higher than observed. Much of this difference can be attributed to precipitation bias and low evaporation rates; further discussion on this matter is presented below.

4.3.2. Comparisons to Observed Streamflow

[50] The observed seasonal runoff cycle (1985–July 1991) at Vicksburg Mississippi is compared to the four simulations in Figure 7. The annual cycle is well represented by simulations using the ERA, CERA, and CNRA forcing. Over the summer and fall periods, these simulations were particularly good with MAEs than 0.05 mm d^{-1}.

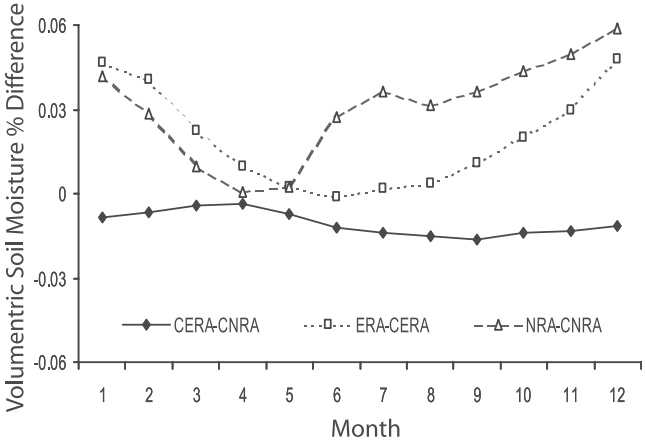

Figure 5. Average (1985–1991) root zone soil moisture differences between the CERA-CNRA, ERA-CERA, and NRA-CNRA simulations for all snow free catchments over North America.

However, during the early spring runoff is overestimated in all three of these simulations, with the ERA exhibiting the most bias. For simulations completed with the NRA forcing, runoff is significantly overestimated in the middle of the year, with the peak being out of phase from observations.

[51] For the simulation of runoff using the CNRA forcing, the bias correction (particularly to precipitation) acts to bring the seasonal cycle of CNRA much closer to reality (r = 0.68 versus 0.29 for the NRA simulation) and allows for a much better approximation of the total runoff flux (Table 2). For the NRA simulation, the timing of the runoff peak (May and June) corresponds to the months of precipitation overestimation. *Lenters et al.* [2000] present similar results for a study using the NRA forcing.

[52] Observed runoff is affected by the various water management practices within the Mississippi River system and the simulated results are impacted by the lack of a streamflow routing methodology. Subsequently, correlations between the modeled and observed runoff are expected to increase if a suitable (catchment based) runoff routing

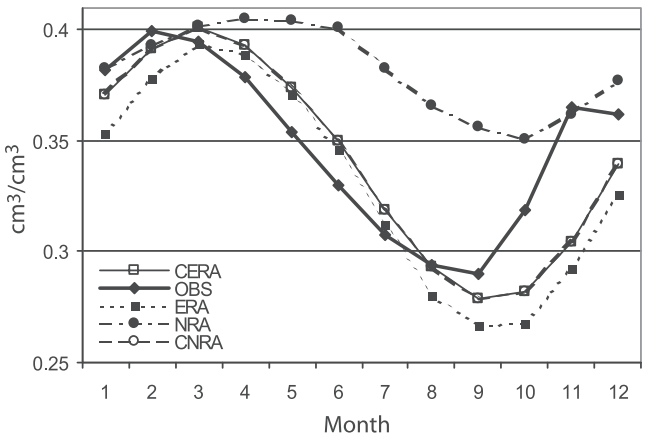

Figure 6. Simulated (CERA, ERA, NRA, and CNRA) and observed (OBS) monthly average volumetric (cm^3 cm^{-3}) soil moisture for three contiguous catchments in southern Illinois (1985–1991).

Table 2. Statistical Comparisons of Each Model Simulation With Observations of Soil Moisture, Runoff, and SWE Expressed in Terms of Correlation and MAE

Observation	Comparison	CERA	ERA	CNRA	NRA
Illinois root zone soil moisture	MAE, cm^3 cm^{-3}	2.3%	2.6%	2.3%	3.0%
	correlation	0.76	0.68	0.76	0.48
Mississippi runoff (mean annual flow 187 mm)	average annual flow	188	200	189	269
	MAE, mm d^{-1}	0.18	0.19	0.17	0.34
	correlation	0.68	0.68	0.68	0.29
Snow depth	MAE, mm mo^{-1}	8.4	13.8	9.2	9.3
	correlation	0.86	0.78	0.93	0.85

scheme is implemented [e.g., *Oki et al.*, 1999]. Therefore the results of the CERA and CNRA simulations are encouraging, as the total volume of flow generated from the basin is in close agreement with observations (Table 2), and months of excessive flow are followed by months of underestimation (Figure 7).

4.3.3. Comparisons to Observed Snow Water Equivalence

[53] Average observed and simulated SWE (1985–1987) for the northern catchments of the Mississippi River basin are shown in Figure 8 and summarized in Table 2. SWE simulated by the CLSM with all of the forcing products are much higher than the SMMR-based observations (although SMMR SWE are typically 10% lower than ground-based observations). In terms of the MAE, simulations using the ERA forcing are higher than the CERA, CNRA, and NRA-based simulations, often overestimating winter SWE by over 100%. For all simulations, peak SWE tends to lag behind observations. Overestimation of the snowpack and rapid melt in the spring helps to explain the tendency for runoff overestimation during the melt season, although some of this error will be mitigated by the introduction of a coupled runoff routing model.

4.3.4. Water Budget Comparisons for Mississippi River Basin

[54] In an attempt to further elucidate the impact of the bias correction on hydrological simulations, components of the annual water budget are shown for the entire Mississippi River basin in Figure 9. Differences between ERA and NRA and GPCP precipitation are presented in Figure 9a. Over the basin, monthly precipitation in the ERA follows the GPCP observations closely for almost all months while

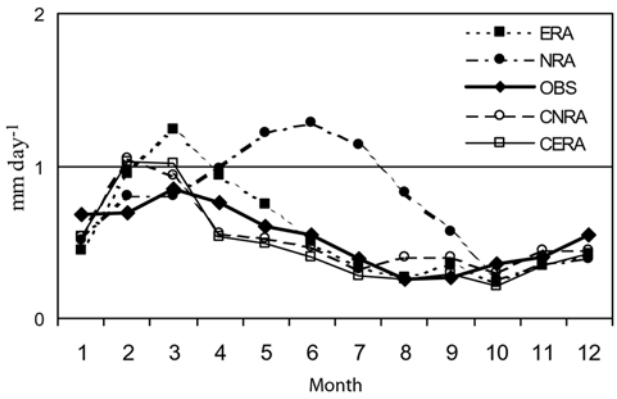

Figure 7. Simulated (CERA, ERA, NRA, and CNRA) and observed (OBS) runoff (mm d^{-1}) for the Mississippi River at Vicksburg, Mississippi (1985–1991).

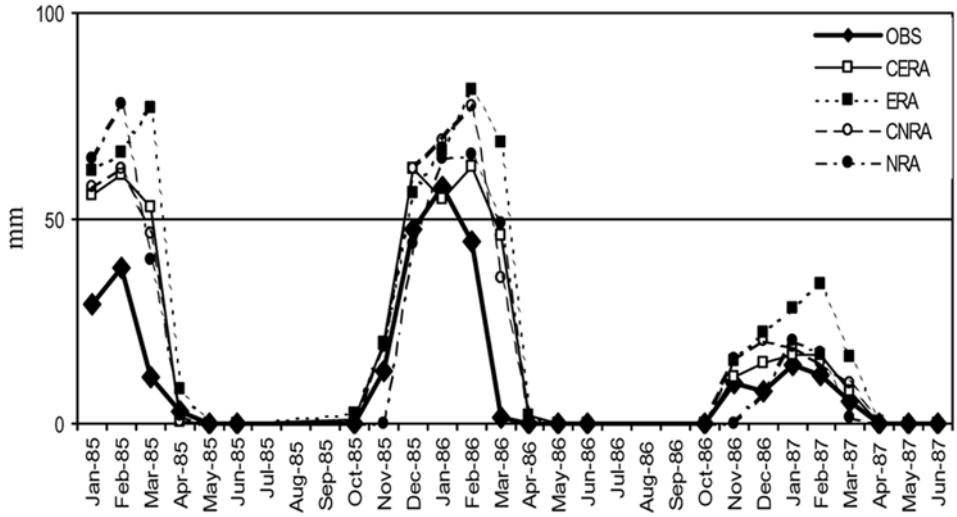

Figure 8. Simulated (CERA, ERA, NRA and CNRA) and observed (OBS) SWE for catchments across the northern Mississippi River Basin (1985–1991).

in the NRA precipitation is greatly overestimated during the summer months. *Roads and Betts* [2000] and *Maurer et al.* [2001a, 2001b] report similar results.

[55] In Figure 9b, we present average monthly total soil column moisture for each of the four simulations. In contrast with the NRA simulation, the annual soil moisture cycle is identical in shape for the ERA, CERA, and CNRA simulations. The NRA simulation predicts peak soil moisture in June, which coincides with the months of high precipitation bias.

[56] Average evapotranspiration for the Mississippi River basin above Vicksburg, Mississippi (see Figure 1), is presented in Figure 9c. Evapotranspiration is greatest for the CERA, CNRA, and ERA simulations and much lower for the NRA simulation. When amounts of evapotranspiration simulated by CLSM with each of the forcing products are compared to the *Roads and Betts* [2000] study, we find that the total amount of evapotranspiration produced from the ERA, CERA, and CNRA simulations are similar to that predicted by the ERA model. However, for the NRA simulations, the situation is reversed and far less evapotranspiration (up to 1 mm d^{-1}) was simulated than in the fully coupled NRA [*Roads and Betts*, 2000; *Lenters et al.*, 2000; *Maurer et al.*, 2001a, 2001b]. In comparisons with FIFE data, *Betts et al.* [1996] found evapotranspiration in the NRA to be suspect because evapotranspiration remained near potential rates despite high relative humidity.

[57] Average (1985–1991) SWE over the Mississippi River basin is presented in Figure 9d. Here the seasonal cycle is similar for the CERA, CNRA, and NRA simulations. In the ERA simulation, the overestimated SWE persists later into the season (this trend was also observed for SWE over the northern catchments of the Mississippi River basin). Overall, the differences observed between the ERA and CERA simulations are due to the temperature bias correction. As illustrated in Figure 2a, there is a strong temperature bias in the ERA data over the interior of the continent extending southward over the northern portion of the Mississippi River basin. Removal of this bias from the ERA forcing allows for greater melt and subsequently lower amounts of snow accumulation within the CERA simulation. In the NRA simulation, the lower amount of SWE observed may be due to lower than observed amounts of winter season precipitation (November–February).

[58] Mississippi River runoff presented in Figure 9e is identical to Figure 7 and is reproduced here for comparison with the other hydrologic fluxes, and discussion here is limited to comparisons between Figure 9e and the other hydrologic variables discussed above. As previously addressed, the bias corrected simulations and the ERA follow the seasonal cycle closely, whereas runoff simulated with the NRA forcing is not in phase with observations. In the ERA simulation, too much runoff is observed over February and March, this is due to higher SWE (Figure 9d), resulting from the negative bias in wintertime temperature (see Figure 2a). In the NRA, differences between the simulated and observed runoff can be attributed to much lower evapotranspiration and excess precipitation (Figure 9a) during the summer months.

5. Summary and Conclusions

[59] One of the main difficulties in producing a large-scale soil moisture data set is the lack of global, temporally and spatially consistent forcing data from which to drive a LSM. Reanalysis products can be used to supply the necessary data, but studies have shown that they are often biased due to errors in the weather models used to create them. Hence the use of the raw reanalysis data to drive LSMs offline will result in inaccurate predictions of the initial state.

[60] In the present study, an attempt to minimize errors in predictions of the initial soil moisture status is realized through a bias reduction scheme to the reanalysis forcing. The bias reduction scheme uses difference- and ratio-based corrections to the NRA (NCEP/NCAR Reanalysis) and ERA (ECMWF Reanalysis) with global observational data sets. Bias corrections were included for the 2-m air and dew point temperatures, short and longwave downwelling radiations, and the precipitation forcing. The sensitivity of the

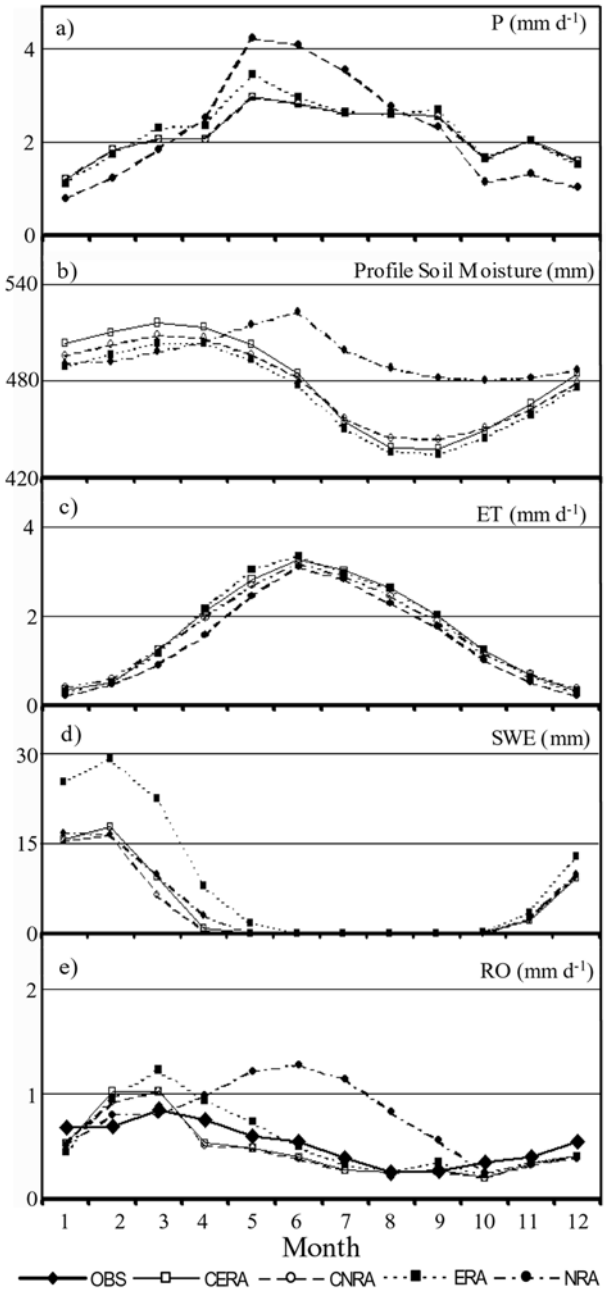

Figure 9. Average monthly differences between the CERA, CNRA, ERA, and NRA simulations for (a) precipitation, (b) evapotranspiration, (c) runoff, (d) profile soil moisture, and (e) snow water equivalence for the Mississippi basin. Basin average runoff observations are included in Figure 9c.

bias correction for initial soil moisture estimation is assessed for simulations completed with the CLSM of *Koster et al.* [2000b], using both the raw and corrected versions of the ERA and NRA forcing.

[61] Overall, the average JJA root zone soil moisture simulated with the ERA, CERA (corrected ERA), and CNRA forcing had similar patterns over much of the North American continent. The same general pattern was also observed in the NRA simulation, but due to bias in the precipitation field, root zone soil moisture conditions are much wetter over the eastern United States extending northward over the Boreal forests of Canada. It is the removal of this bias in the CNRA forcing that accounts for most of the difference between the CNRA and NRA simulation results.

[62] Potential improvements to hydrological simulations because of the bias correction are evaluated through comparisons with observations over the Mississippi River basin. In comparisons with soil moisture, runoff, and SWE observations, the CERA and CNRA simulation results were found to be in close agreement. In contrast, the simulations produced with ERA and NRA forcing data are not always as accurate. The precipitation and high humidity bias to the NRA forcing leads to soil moisture and runoff estimations that are out of phase with observations. Although the ERA simulations of soil moisture are much closer to the CERA and CNRA simulations, over winter the negative temperature bias perpetuates excess storage of snow, subsequently producing overly high runoff volumes during the early spring.

[63] This study has demonstrated that the implementation of a simple bias reduction scheme reduces errors in the simulation of soil moisture, runoff, and SWE. While this is an encouraging result, there exists the possibility for further improvement by refinement of the bias correction procedures described above. Recent work by *Berg and Famiglietti* [2003] demonstrates that despite the bias correction there will remain some uncertainty in the initial soil moisture estimate. Of particular importance is treatment of variability at the submonthly timescale. Therefore modifications to the procedures outlined above that incorporate additional statistics such as wet day frequency or mean minimum and maximum temperatures can improve the forcing product described.

[64] Based on the results of this study, we anticipate that the value of soil moisture initializations completed using the corrected forcing products are closer to actual surface conditions and subsequently more useful to the climate modeling community. Hence it is possible to increase the accuracy of simulations for the initial soil moisture state using reanalysis products after the implementation of a relatively simple bias reduction procedure.

[65] **Acknowledgments.** This work was supported by NASA grants NAG5-11645, 12344, and the NASA Earth Science Fellowship Program. We would also like to acknowledge the comments and insights of three anonymous reviewers. The support of NCEP/NCAR is acknowledged for technical assistance and for providing the reanalysis data used in this study. Sally Holl assisted in the interpolation of the snow depth fields.

References

Atlas, R., N. Wolfson, and J. Terry, The effects of SST and soil moisture anomalies on GCM model simulations of the 1988 U.S. summer drought, *J. Clim.*, *6*, 2034–2048, 1993.

Berg, A. A., and J. S. Famiglietti, Characterizing regional uncertainty in the initial soil moisture status, *Geophys. Res. Lett.*, *30*(9), 1466, doi:10.1029/2003GL017015, 2003.

Betts, A. K., S.-Y. Hong, and H.-L. Pan, Comparison of NCEP/NCAR reanalysis with 1987 FIFE data, *Mon. Weather Rev.*, *124*, 1480–1498, 1996.

Betts, A. K., P. Viterbo, and A. C. M. Beljaars, Comparison of the ECMWF reanalysis with the 1987 FIFE data, *Mon. Weather Rev.*, *126*, 186–198, 1998a.

Betts, A. K., P. Viterbo, A. C. M. Beljaars, H.-L. Pan, S.-L. Hong, M. Goulden, and S. Wofsy, Evaluation of land-surface interaction in

ECMWF and NCEP/NCAR reanalysis models over grassland (FIFE) and boreal forest (BOREAS), *J. Geophys. Res.*, *103*, 23,079–23,085, 1998b.

Betts, A. K., P. Viterbo, and E. Wood, Surface energy and water balance for the Arkansas-Red River basin from the ECMWF reanalysis, *J. Clim.*, *11*, 2881–2897, 1998c.

Bounouna, L., and T. N. Krishnamurti, Influence of soil moisture on Sahelian climate prediction I, *Meteorol. Atmos. Phys.*, *52*, 183–203, 1993a.

Bounouna, L., and T. N. Krishnamurti, Influence of soil moisture on Sahelian climate prediction II, *Meteorol. Atmos. Phys.*, *52*, 205–224, 1993b.

Chang, A., Nimbus-7 SMMR Global Monthly Snow Cover and Snow Depth, Natl. Snow and Ice Data Cent., Digital Media, Boulder, Colo., 1995.

Chang, A. T. C., J. L. Foster, and D. K. Hall, Nimbus-7 SMMR derived global snow cover parameters, *Ann. Glaciol.*, *9*, 39–44, 1987.

Chang, A. T. C., J. L. Foster, D. K. Hall, H. W. Powell, and Y. L. Chien, Nimbus-7 SMMR Derived Global Snow Cover and Snow Depth Data Set, The Pilot Land Data Syst., NASA/Goddard Space Flight Cent., Greenbelt, Md., 1992.

Delworth, T., and S. Manabe, Climate variability and land surface processes, *Adv. Water Resour.*, *16*, 3–20, 1993.

Dirmeyer, P. A., Using a global soil wetness dataset to improve seasonal climate simulation, *J. Clim.*, *13*, 2900–2922, 2000.

Dirmeyer, P. A., A. J. Dolman, and N. Sato, The pilot phase of the global soil wetness project, *Bull. Am. Meteorol. Soc.*, *80*, 851–878, 1999.

Douvill, H., and F. Chavin, Relevance of soil moisture for seasonal climate predictions: A preliminary study, *Clim. Dyn.*, *16*, 719–736, 2000.

Ducharne, A., and K. Laval, Influence of the realistic description of soil water-holding capacity on the global water cycle in a GCM, *J. Clim.*, *13*, 4393–4413, 2000.

Ducharne, A., R. D. Koster, M. J. Suarez, M. Stieglitz, and P. Kumar, A catchment-based approach to modeling land surface processes in a general circulation model: 2. Parameter estimation and model demonstration, *J. Geophys. Res.*, *105*, 24,823–24,838, 2000.

Famiglietti, J. S., and E. F. Wood, Evapotranspiration and runoff from large land areas: Land surface hydrology for atmospheric general circulation models, *Surv. Geophys.*, *12*, 179–204, 1991.

Famiglietti, J. S., and E. F. Wood, Multi-scale modeling of spatially-variable water and energy balance processes, *Water Resour. Res.*, *30*, 3061–3078, 1994.

Fennessy, M. J., and J. Shukla, Impact of initial soil wetness on seasonal atmospheric prediction, *J. Clim.*, *12*, 3167–3180, 1999.

Gesch, D. B., K. L. Verdin, and S. K. Greenlee, New land surface digital elevation model covers the Earth, *Eos Trans. AGU*, *80*(6), 69–70, 1999.

Gibson, J. K., P. Kållberg, S. Uppala, A. Nomura, A. Hernandez, and E. Serrano, ERA Description, *ECMWF Reanal. Proj. Rep. Ser. 1*, 72 pp., Eur. Cent. For Medium-Range Weather Forecasts, Reading, England, 1997.

Gupta, S. K., N. A. Ritchey, A. C. Wilber, C. H. Whitlock, G. G. Gibson, and P. W. Stackhouse Jr., A climatology of surface radiation budget derived from satellite data, *J. Clim.*, *12*, 2691–2710, 1999.

Hollinger, S. E., and S. A. Isard, A soil moisture climatology of Illinois, *J. Clim.*, *7*, 822–833, 1994.

Hong, S.-Y., and H.-L. Pan, Non local boundary layer vertical diffusion in a medium-range forecast model, *Mon. Weather Rev.*, *124*, 2322–2339, 1996.

Houser, P., W. Shuttleworth, J. S. Famiglietti, H. Gupta, K. Syed, and D. Goodrich, Integration of soil moisture remote sensing and hydrologic modeling using data assimilation, *Water Resour. Res.*, *34*, 3405–3420, 1998.

Huffman, G. J., R. F. Adler, P. Arkin, A. Chang, R. Ferraro, A. Gruber, J. Janowiak, A. McNab, B. Rudolf, and U. Schneider, The Global Precipitation Climatology Project (GPCP) combined precipitation dataset, *Bull. Am. Meteorol. Soc.*, *78*, 5–20, 1997.

Jackson, T. J., D. M. LeVine, A. Y. Hsu, A. Oldak, P. J. Starks, C. T. Swift, J. D. Isham, and M. Haken, Soil moisture mapping at regional scales using microwave radiometry: The southern great plains hydrology experiment, *IEEE Trans. Geosci. Remote Sens.*, *37*, 2136–2151, 1999.

Jensen, M. E., R. D. Burman, and R. G. Allen, *Evapotranspiration and Irrigation Water Requirements: A Manual*, *ASCE Manuals Rep. Eng. Pract.*, vol. 70, 332 pp., Am. Soc. Civ. Eng., New York, 1990.

Kalnay, E., et al., The NCEP/NCAR 40-year reanalysis project, *Bull. Am. Meteorol. Soc.*, *77*, 437–471, 1996.

Koster, R. D., and M. J. Suarez, Modeling the land surface boundary in climate models as a composite of independent vegetation stands, *J. Geophys. Res.*, *97*, 2697–2715, 1992.

Koster, R. D., and M. J. Suarez, The influence of land surface moisture retention on precipitation statistics, *J. Clim.*, *9*, 2551–2567, 1996a.

Koster, R. D., and M. J. Suarez, Energy and water balance calculations in the mosaic LSM, *NASA Tech. Memo., 104606*, vol. 9, 76 pp., 1996b.

Koster, R. D., M. J. Suarez, and M. Heiser, Variance and predictability of precipitation at seasonal to interannual timescales, *J. Hydrometeorol.*, *1*, 26–46, 2000a.

Koster, R. D., M. J. Suarez, A. Ducharne, M. Stieglitz, and P. Kumar, A catchment-based approach to modeling land surface processes in a general circulation model: 1. Model structure, *J. Geophys. Res.*, *105*, 24,809–24,822, 2000b.

Legates, D. R., and C. J. Willmott, Mean seasonal and spatial variability global surface air temperature, *Theor. Appl. Climatol.*, *41*, 11–21, 1990.

Lenters, J. D., M. T. Coe, and J. A. Foley, Surface water balance of the continental United States, 1963–1995: Regional evaluation of a terrestrial biosphere model and the NCEP/NCAR reanalysis, *J. Geophys. Res.*, *105*, 22,393–22,425, 2000.

Lynch-Stieglitz, M., The development and validation of a simple snow model for the GISS GCM, *J. Clim.*, *7*, 1842–1855, 1994.

Maurer, E. P., G. M. O'Donnell, D. P. Lettenmaier, and J. O. Roads, Evaluation of the land surface water budget in NCEP/NCAR and NCEP/DOE reanalyses using an off-line hydrologic model, *J. Geophys. Res.*, *106*, 17,841–17,862, 2001a.

Maurer, E. P., G. M. O'Donnell, D. P. Lettenmaier, and J. O. Roads, Evaluation of NCEP/NCAR reanalysis water and energy budgets using macroscale hydrologic model simulations, in *Land Surface Hydrology, Meteorology and Climate: Observations and Modeling*, *Water Sci. Appl.*, vol. 3, edited by L. Venkataraman, J. Albertson, and J. Schaake, pp. 137–158, AGU, Washington, D. C., 2001b.

Milly, P. C. D., and K. A. Dunne, Sensitivity of global water cycle to the water holding capacity of land, *J. Clim.*, *7*, 506–526, 1994.

New, M., M. Hulme, and P. Jones, Representing twentieth-century space-time climate variability, part II, Development of 1901–96 monthly grids of terrestrial surface climate, *J. Clim.*, *13*, 2217–2238, 2000.

Njoku, E. G., and D. Entekhabi, Passive microwave remote sensing of soil moisture, *J. Hydrol.*, *184*, 101–129, 1996.

Oglesby, R. J., Springtime soil moisture, natural climate variability and North American drought as simulated by the NCAR community Model 1, *J. Clim.*, *4*, 890–897, 1991.

Oki, T., T. Nishimura, and P. Dirmeyer, Assessment of annual runoff from land surface models using total integrating pathways (TRIP), *J. Meteorol. Soc. Jpn.*, *77*, 235–255, 1999.

Owe, M., and A. A. Van de Griend, Comparison of soil moisture penetration depths for several bare soils at two microwave frequencies and implications for remote sensing, *Water Resour. Res.*, *34*, 2319–2327, 1998.

Owe, M., R. de Jeu, and J. P. Walker, A methodology for surface soil moisture and vegetation optical depth retrieval using the microwave polarization difference index, *IEEE Trans. Geosci. Remote Sens.*, *39*, 1643–1654, 2001.

Reichle, R. H., D. B. McLaughlin, and D. Entekhabi, Variational data assimilation of microwave radiobrightness observations for land surface hydrology applications, *IEEE Trans. Geosci. Remote Sens.*, *39*, 1708–1718, 2001.

Roads, J., and A. Betts, NCEPP-NCAR and ECMWF reanalysis surface water and energy budgets for the Mississippi basin, *J. Hydrometeorol.*, *1*, 88–94, 2000.

Robock, A., K. Y. Vinnikov, G. Srinivasan, J. K. Entin, S. E. Hollinger, N. A. Speranskaya, S. Liu, and A. Namkhai, The global soil moisture data bank, *Bull. Am. Meteorol. Soc.*, *81*, 1281–1299, 2000.

Rodell, M., and J. S. Famiglietti, Detectability of variations in continental water storage from satellite observations of the time dependent gravity field, *Water Resour. Res.*, *35*, 2705–2723, 1999.

Row, L. W., D. A. Hastings, and P. K. Dunbar, *TerrainBase Worldwide Digital Terrain Data Doc. Manual*, Natl. Geophys. Data Cent., Boulder, Colo., 1995.

Sellers, P. J., Y. Mintz, Y. C. Sud, and A. Dalcher, A simple biosphere model (SiB) for use within general circulation models, *J. Atmos. Sci.*, *43*, 505–531, 1986.

Sellers, P. J., et al., The ISLSCP initiative I global datasets: Surface boundary conditions and atmospheric forcings for land-atmosphere studies, *Bull. Am. Meteorol. Soc.*, *77*, 1987–2006, 1996.

Stieglitz, M., D. Rind, J. Famiglietti, and C. Rosenzweig, An efficient approach to modeling the topographic control of surface hydrology for regional and global climate modeling, *J. Clim.*, *10*, 118–137, 1997.

Stieglitz, M., A. Ducharne, R. Koster, and M. Suarez, The impact of detailed snow physics on the simulation of snow cover and subsurface thermodynamics at continental scales, *J. Hydrometeorol.*, *2*, 228–242, 2001.

Verdin, K. L., and J. P. Verdin, A topological system for delineation and codification of the Earth's river basins, *J. Hydrol.*, *218*, 1–12, 1999.

Walker, J. P., and P. R. Houser, A methodology for initializing soil moisture in a global climate model: Assimilation of near-surface soil moisture observations, *J. Geophys. Res.*, *106*, 11,761–11,774, 2001.

Walker, J. P., G. R. Willgoose, and J. D. Kalma, One-dimensional soil moisture profile retrieval by assimilation of near-surface measurements: A simplified soil moisture model and field application, *J. Hydrometeorol.*, *2*, 356–373, 2001.

Wild, M., A. Ohmura, and H. Gilgen, The distribution of solar energy at the Earth's surface as calculated in the ECMWF reanalysis, *Geophys. Res. Lett.*, *25*, 4373–4376, 1998.

Xue, Y., and J. Shukla, The influence of land surface properties on Sahel climate, part I, Desertification, *J. Clim.*, *6*, 2232–2345, 1993.

A. A. Berg and J. S. Famiglietti, Department of Earth System Science, University of California at Irvine, 230 Rowland Hall, Irvine, CA 92687-3100, USA. (berga@uci.edu; jfamigli@uci.edu)

P. R. Houser, Hydrological Sciences Branch, NASA Goddard Space Flight Center, Greenbelt, MD 20771, USA. (houser@dao.gsfc.nas)

J. P. Walker, Department of Civil and Environmental Engineering, University of Melbourne, Parkville, Victoria 3010, Australia. (J.walker@unimelb.edu.au)